Nanoscale

Accepted Manuscript

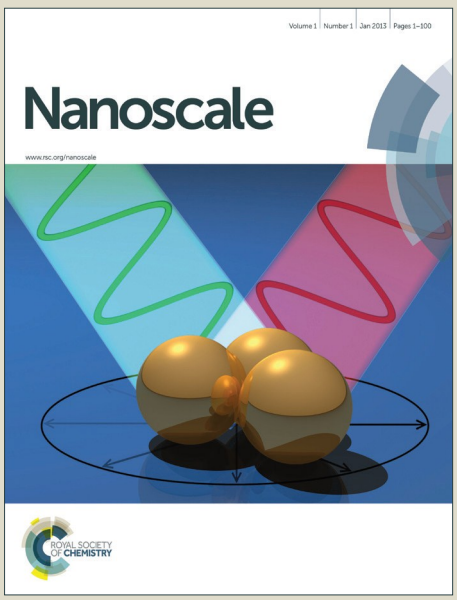

ROYAL SOCIETY OF CHEMISTRY

www.rsc.org/nanoscale

Double Fano resoances in plasmonic nanocross molecules and magnetic plasmon propagation

Guo-Zhou Li,[a] Qiang Li[b] and Li-Jun Wu*[a]

[a]*Guangdong Provincial Key Laboratory of Nanophotonic Functional Materials and Devices, School of Information and Optoelectronic Science and Engineering, South China Normal University, Guangzhou 510006, P.R. China. E-mail: ljwu@scnu.edu.cn*

[b]*Department of Physics, Hong Kong University of Science and Technology, Clear Water Bay, Kowloon, Hong Kong, P.R. China.*

Abstract Double Fano resonances in optical frequency are investigated in an artificial plasmonic molecule consisting of seven identical nanocrosses. These two Fano resonances are found to originate from different physical mechanisms. One is caused by the excitation of the inherent quadrupole dark mode supported by the single nanocross, and the other is attributed to the magnetic plasmon mode due to the generation of antiphase ring currents in adjacent fused tetramers. The two Fano resonances can either be tuned simultaneously or independently within a wide spectral range by adjusting the geometrical parameters of the nanocrosses. The excitation of the magnetic plasmon in a chain made of coupled nanoparticles allows for subwavelength guiding of optical energy with low radiative losses. The field decay length is as long as 2.608 μm, which is comparable to that of the magnetic plasmon waveguides and far surpasses the value achieved in electric plasmon counterparts. Because of the special shape of the nanocross, a Mach-Zehnder interferometer can be built to steer optical beams. These results show that the proposed plasmonic nanostructures have potential applications in biochemical sensing, narrow line-shape engineering and on-chip optical signal propagation in nanoscale integrated optics.

Keywords: Fano resonances, magnetic plasmons, nanocluster, plasmon waveguide

1 Introduction

The collective oscillation of the conduction electrons of a metallic nanoparticle (NP) can give rise to localized surface plasmon resonances (LSPRs), which are highly sensitive to the variation of the nanoparticle's size, shape, and surrounding medium.[1,2] In a hybrid structure composed of NPs, surface plasmon (SP) coupling can create strong fields mainly concentrated in gaps among NPs, known as "hot spots". One of the simplest examples is a dimer comprised two gold nanoparticles. When the two NPs are positioned into close proximity, their plasmons mix and hybridize, resulting in the formation of bonding and antibonding plasmon modes.[3] The plasmon hybridization theory can provide an intuitive picture to understand the optical properties of metallic nanostructures with complex geometries by analogy to molecular orbitals.[4-6] Inspired by the configuration and constitution of organic compounds in biology and chemistry, artificial plasmonic molecules which are much smaller than operation wavelength, have attracted lots of attention due to their novel electromagnetic properties in recent years.[7-8]

Recently, Fano resonances in plasmonic nanostructures which arise from the destructive interference between a broad superradiant and a narrow subradiant mode, have attracted many researchers' attention due to the narrow and characteristic asymmetric lineshape spectrally. Fano resonances have been reported in various plasmonic systems. For instance, plasmonic nanoparticle clusters consisting of three or more nanoparticles,[9-13] dolmen-type slab structure[14-18] and nonconcentric ring/disk nanocavity[19-20] have shown Fano resonances in optical regime. Plasmonic Fano resonances have emerged as new methods to not only enhance light-matter interaction, but also promise for many potential applications such as biochemical sensor,[21] slow light,[17] and surface enhanced Raman scattering (SERS).[22] Compared to a single Fano resonance, the plasmon lineshape of multiple Fano resonances can be tuned at several spectral positions simultaneously. Thus they have gained much attention.[23-34] For example, multiple Fano resonances have been applied for multiwavelength biosensing,[19] three dimensional ruler,[35] and highly directional on-chip antenna,[36] etc. However, most of the reported multiple Fano resonances are a direct result of the collective behavior of the total plasmonic systems[11,18,26] and thus the individual Fano resonance cannot be tuned independently which will limit their applications.

In nanoscale integrated optics, it is highly desirable that optical frequency signals can be coupled to and propagated along plasmonic structures. Due to significant radiation loss, the propagation distance of electric plasmons along a chain is restricted to a few hundred nanometers.[37,38] Fortunately, the radiation loss of a magnetic dipole, which can be realized in artificial plasmonic molecules in the optical frequency,[39,40] is considerably lower compared to that of an electric dipole of similar dimension.[41] However, there are very few reported nanostructures supporting magnetic plasmon modes. Recently, a conjugated heptamers structure with two shared gold disks has been proposed to support magnetic plasmon mode. Its chain has been utilized to realize long-range magnetic plasmon propagation.[7, 8]

In this article, we propose a heptamer composed of seven nanocrosses to generate double Fano resonances. Due to the geometric adjustability of the nanocross unit cell,[42,43] our proposed plasmonic nanostructure can afford more degree of freedom to tune its optical responses. We find the two Fano resonances are based on different physical mechanisms. One Fano resonance results from the excitation of the dark quadrupole mode in the nanocross, and the other is originated from the excitation of the magnetic plasmon mode which is a collective mode of the heptamer configuration. Consequently, the lineshape of the double Fano resonances can either be tuned simultaneously or independently by

changing the length and width of the nanocross arm, the angle between the arms, and the gap between neighbor nanocrosses. We further show that the magnetic plasmon can efficiently propagate along a long chain of the proposed structure when excited by a dipole source. Due to strong near-field interaction, the magnetic moments induced by the alternative ring currents are aligned in a complete antiparallel manner, which can substantially reduce the radiation dissipation. This special plasmonic structure can be utilized to build a Mach-Zehnder interferometer to split and combine propagating magnetic plasmons.[8] Our proposed magnetic plasmon waveguide exhibits a field decay length of 2.608 μm, which is comparable to that of the magnetic plasmon waveguides proposed in previous papers [7,8] and far surpasses the value achieved in electric plasmon counterparts.[44-46] These results show that our proposed plasmonic nanostructures have potential applications in biosensing, nanometric-scale energy transport, information processing, and data storage, etc.

2 Results and discussions

2.1 Double Fano resoances in plasmonic nanocross molecules

The schematic of our proposed heptamer consists of a central nanocross surrounded by a ring of six adjacent satellites, as shown in Fig. 1(a). The geometric parameters cross length *l*, width *W*, thickness *H*, and cross arm angle α are 370 nm, 70 nm, 50 nm, and 60 °, respectively. The gap *S* between neighbor arms is chosen to be 30 nm. A commercial finite element method (COMSOL multiphysics) is implemented to acquire the spectra, field and surface current distributions. For simplicity, the substrate is not included in the simulations because it does not change the underlying physics and only slightly affects the spectral response. The background with refractive index of 1.33 is taken into account. For the dielectric permittivity of gold, we use a Drude model which shows good agreement with the experimental data reported in literature.[47]

The extinction spectra of a single nanocross with different excitations are shown in Fig. 1(b). All the excitation is *y*-polarized in the paper. The black line corresponds to the nonretarded case where the *y*-polarized light is normally incident from the top. Only a broad resonance is observed at 1715 nm. When the illumination is from the side at grazing incidence (red line), an additional narrow resonance is excited at 1310 nm. The charge density distributions in the insets of Fig. 1(b) reveal the nature of the dipolar (black dot) and quadrupolar (red dot) mode. The dimension of the nanocross is designed to allow for phase retardation. Thus the field gradient along the structure can couple to higher order mode which is dark for normal incidence.[42,43]

The extinction, scattering and absorption spectra of the plasmonic heptamer composed of seven nanocrosses are shown in Fig. 2(a) under normal incidence illumination. Two clear dips are observed in the scattering spectrum at 1340 nm and 2200 nm, respectively. The first absorption enhancement at 1310 nm can be attributed to the subradiant quadrupole mode because it is at the same spectral position as the aforementioned quadrupole mode of the single nanocross (refer to Fig. 1(b)). Fig. 2(b) exhibits the electric field and current vector distributions at 1310 nm. We can observe very strong field enhancement on the left and the right side nanocross, revealing the occurrence of the dark quadrupole mode. The current vector distributions further confirm the nature of the dark quadrupole mode. On the other hand, when the dipolar components of all constituent nanoparticles are oriented in phase, there is also an overlapped superradiant bright mode according to the plasmon hybridization theory. Therefore, the first Fano resonance (FR1) at 1310 nm can be attributed to the destructive interference between the overlapped bright dipole and the dark quadrupole mode. The second resonance (FR2) at 2170 nm is

distinct from the first one, which is to be emphasized in the following context. From its current vector distribution presented in Fig. 2(c), we can observe that the resonance is associated with an excitation of two circular currents which flow in opposite directions around the two fused tetramers. The shared nanocross works as a mutual current link. The corresponding magnetic field component *Hz* superimposed in Fig. 2(c) more explicitly uncovers the excitation of two antiparellel magnetic dipoles moment in the individual heptamer, similar to the behavior in a conjugated heptamers cluster.[7,8] These results demonstrate that FR2 can be attributed to the interaction between electric dipoles and magnetic dipoles resonance. The presence of the central nanocross is a key factor to control FR2. Strong near-field enhancement is localized in interparticle gaps due to the almost complete suppression of radiation damping as presented in Fig. 2(d).

The tunability of plasmonic structures is highly desirable in many applications. Most of the multiple Fano resonances, however, can only be tuned simultaneously. In our proposed structure, we can adjust the double Fano resonances independently by varying the geometric parameters of the nanocross heptamer because of their different underlying physical mechanisms.

For FR1, the position of the resonance peak is mainly determined by the aspect ratio, l/W.[43] As shown in Fig. 3(a), FR1 blueshifts as largely as 400 nm (from 1500 nm to 1100 nm) with an increase of the nanocross arm width W (from 30 nm to 150 nm) while FR2 almost remains constant due to the concentration of the surface charges near the apexes. FR2 is actually similar in nature to an inductive capacitive (LC) resonance since both of them give rise to localized current configurations that result in a magnetic dipole moment perpendicular to the structure plane. The resonance frequency $\omega_0 = 1/\sqrt{LC}$, in which L is the induction of the arm and C the capacitance of the gap. An increase of the gap between neighbor nanocrosses S corresponds to a decrease of the capacitance C and a blueshift of the resonance. This can be observed in Fig. 3(b). When S is increased from 10 nm to 100 nm, the position of FR2 changes from 2800 nm to 1900 nm. Meanwhile, the spectral position of FR1 almost remains constant except the depth modulation decreases slightly due to the weaker coupling.

On the other hand, the modulation depth of the double Fano resonance can also be tuned in our proposed structure. Fig. 3(c) exhibits the influence of the angle α between two arms in the unit cell. As seen, the spectral position of the double Fano resonances does not change a lot, but the depth modulation of FR2 decreases and some higher order plasmon modes (not analyzed here) appear with an increase of α. The possible reason for the insensitivity of the FR1 response is that the quadrupole mode does not change much in a wide angular range which has been noted in a previous report.[43] For FR2, when the angle α is decreased, the superradiant mode of the heptamer (related to the dipole mode of an individual cross) redshifts[43] and gradually starts to spectrally overlap with the subradiant magnetic mode. The stronger the spectral overlap, the deeper the spectral dip related to the Fano interference.

Of course, the double Fano resonances can also be tuned simultaneously by varying other geometric parameters. For example, when the length of the nanocross arm l is increased, both FR1 and FR2 exhibit obvious redshifts as illustrated in Fig. 3(d). But the modulation depth does not vary a lot. The reason for the redshift of FR1 is because the spectral position of the quadrupole mode in a nanocross is proportional to the arm length l.[43] Analogue to the LC resonance, the increase of the arm length l leads to an increase of the nanocross induction and thus FR2 redshifts.

2.2 Magnetic plasmon propagation along coupled nanoparticle chains

Strong radiation loss has been one of the major obstacles for utilizing metallic nanoparticle chains as

plasmonic waveguides. The radiation loss of a magnetic dipole is substantially lower compared to that of an electric dipole.[41] It may provide another feasible route to transport energy in nanosized systems. Here we investigate the magnetic plasmon propagation along a finite chain of connected tetramers based on the proposed nanocross as presented in Fig. 4(a). The chain size is chosen to be 12 tetramers. The magnetic plasmon is excited by a dipole source placed at a distance of 150 nm away from the left end of the chain. The current vector distribution and magnetic field component (*Hz*) at the selected resonant wavelength (2030 nm) are displayed in Fig. 4(a). As shown, the ring currents generated in the first tetramer are split into an upper and lower branch via mutual current links, and flow along two separate optical paths with the same phase. It is followed by converging at the center of the third tetramer with constructive interference. The induced magnetic dipole moments are aligned in an alternatively antiparallel fashion, behaving like "antiferromagnetism" as shown in the bottom inset of Fig. 4(a). The magnetic plasmons then continue to propagate forward in a repeated manner. This constitutes a plasmonic Mach-Zehnder interferometer, which can be used for splitting beam in nanoscale integrated optics. In order to quantify the efficiency of the magnetic plasmon waveguide, we calculate the time-averaged energy flow along the chain. In the calculation process, the first and the last tetramer units have been excluded from the calculation to minimize the interference effects due to their light scattering. The exponential fit yields a field decay length of 2.608 μm as shown in Fig. 4(b), which corresponds to 8.7 unit cells or 1.3 free space wavelengths. This decay length is comparable to a recently reported result of 2.65μm (5.2 unit cells or 2 free space wavelengths) in a magnetic plasmon based system.[7] In a closely spaced metallic nanoparticles linear chain, the electric plasmon propagation at 520 nm has a decay length of 410 nm, which corresponds to 5.4 unit cells or 0.8 free space wavelengths.[44] The superior performance of the magnetic plasmon propagation results from much stronger field concentration compared to electric plasmon mode as well as the subradiant nature of the magnetic ring mode, which is weakly coupled to far-field radiation. The performance of the plasmonic waveguide can be further improved either by scaling down the dimension reasonably or using other exciting sources (see supplementary information). The result clearly illustrates that the magnetic plasmon is a highly promising candidate for future energy transport components and devices.

3 Conclusions

In summary, we have demonstrated that double Fano resonances can be achieved in an artificial plasmonic molecule made of seven identical nanocrosses. These two Fano resonances are found to originate from two different physical mechanisms. One is caused by the excitation of the inherent quadrupole mode supported by the constituent nanocross, and the other is originated from a magnetic plasmon mode composed of two opposite current loops. Due to this reason, the double Fano resonances can either be tuned independently or simultaneously within a wide range by adjusting the geometrical parameters of the system, such as the width and length of the nanocross arm, the gap between neighbor nancrosses and the angle between the arms. Furthermore, we examined the propagation of the magnetic plasmons along a long chain, and found that these structures can support low-loss propagation with a long field decay length due to the subradiant nature of the magnetic plasmons. One can incorporate a gain medium such as quantum dots and optimize structure to further improve the performance. A plasmonic Mach-Zehnder interferometer can also be realized because of the unique characteristic of the proposed nanocross. Our proposed structures show potential applications not only in multiple wavelength biosensing, but also in narrow line-shape engineering and on-chip optical signal

propagation at nanoscale.

Acknowledgements

The authors acknowledge the financial support from National Natural Science Foundation of China (Grant No. 61378082) and the Project of High-level Professionals in the Universities of Guangdong Province.

Notes and References

1 S. A. Maier, *Plasmonics: Fundamentals and Applications*, Springer, 2007.
2 W. L. Barnes, A. Dereux and T. W. Ebbesen, *Nature*, 2003, **424**, 824-830.
3 J. B. Lassiter, J. Aizpurua, L. I. Hernandez, D. W. Brandl, I. Romero, S. Lal, J. H. Hafner, P. Nordlander and N. J. Halas, *Nano Lett.*, 2008, **8**, 1212–1218.
4 P. Nordlander, C. Oubre, E. Prodan, K. Li and M. I. Stockman, *Nano Lett.*, 2004,**4**, 899-903.
5 P. Nordlander and E. Prodan, *Nano Lett.*, 2004, **4**, 2209-2213.
6 H. Wang, D. W. Brandl, F. Le, P. Nordlander and N. J. Halas, *Nano Lett.*, 2006, **6**, 827-832.
7 N. Liu, S. Mukherjee, K. Bao, L. V. Brown, J. Dorfmueller, P. Nordlander and N. J. Halas, *Nano Lett.*, 2012, **12**, 364–369.
8 N. Liu, S. Mukherjee, K. Bao, Y. Li, L. V. Brown, P. Nordlander and N. J. Halas, *ACS Nano*, 2012, **6**, 5482–5488.
9 J. A. Fan, C. Wu, K. Bao, J. Bao, R. Bardhan, N. J. Halas, V. N. Manoharan, P. Nordlander, G. Shvets and F. Capasso, *Science*, 2010, **328**, 1135−1138.
10 J. Sancho-parramon and S. Bosch, *ACS Nano*, 2012, **6**, 8415−8423.
11 M. Hentschel, D. Dregely, R. Vogelgesang, H. Giessen and N. Liu, *ACS Nano*, 2011, **5**, 2042−2050.
12 J. A. Fan, K. Bao, C. Wu, J. Bao, R. Bardhan, N. J. Halas, V. N. Manoharan, G. Shvets, P. Nordlander and F. Capasso, *Nano Lett.*, 2010, **10**, 4680−4685.
13 S. Liu, Z. Yang, R. Liu and X. Li, *ACS Nano*, 2012, **6**, 6260−6271.
14 N. Verellen, Y. Sonnefraud, H. Sobhani, F. Hao, V. Moshchalkov, P. V. Dorpe, P. Nordlander, S. A. Maier and V. V. Moshchalkov, *Nano Lett.*, 2009, **9**, 1663−1667.
15 S. H. Mousavi, I. Kholmanov, K. B. Alici, D. Purtseladze, N. Arju, K. Tatar, D. Y. Fozdar, J. W. Suk, Y. Hao and A. B. Khanikaev, *Nano Lett.*, 2013, **13**,1111−1117.
16 B. Gallinet, T. Siegfried, H. Sigg, P. Nordlander and O. J. F. Martin, *Nano Lett.*, 2013, **13**, 497−503.
17 S. Zhang, D. A. Genov, Y. Wang, M. Liu and X. Zhang, *Phys. Rev. Lett.*, 2008, **101**,047401.
18 C. Wu, A. B. Khanikaev and G. Shvets, *Phys. Rev. Lett.*, 2011, **106**, 107403.
19 Y. H. Fu, J. B. Zhang, Y. F. Yu and B. Luk'yanchuk, *ACS Nano*, 2012, **6**, 5130−5137.
20 F. Hao, P. Nordlander, Y. Sonnefraud, P. Van Dorpe and S. A. Maier, *ACS Nano*, 2009, **3**, 643−652.
21 G. Li, Q. Li, L. Xu and L. Wu, *Plasmonics*, 2015, **10**, doi: 10.1007/s11468-015-9947-9.
22 F. S. Ou, M. Hu, I. Naumov, A. Kim, W. Wu, A. M. Bratkovsky, X. Li, R. S. Williams and Z. Li, *Nano Lett.*, 2011, **11**, 2538–2542.
23 J. Chen, Q. Shen, Z. Chen, Q. Wang, C. Tang and Z. Wang, *J. Chem. Phys.*, 2012, **136**, 214703-214709.
24 D. Dregely, M. Hentschel and H. Giessen, *ACS Nano*, 2011, **5**, 8202-8211.
25 Y. Cui, J. Zhou, V. A. Tamma and W. Park, *ACS Nano*, 2012, **6**, 2385-2393.

26 S. D. Liu, Z. Yang, R. P. Liu and X. Y. Li, *ACS Nano*, 2012, **6**, 6260-6271.
27 S. D. Liu, Y. B. Yang, Z. H. Chen, W. J. Wang, H. M. Fei, M. J. Zhang and Y. C. Wang, *J. Phys. Chem. C*, 2013, **117**, 14218-14228.
28 Y. Wang, Z. Li, K. Zhao, A. Sobhani, X. Zhu, Z. Fang and N. J. Halas, *Nanoscale*, 2013, **5**, 9897-9901.
29 Z. J. Yang, Q. Q. Wang and H. Q. Lin, *Appl. Phys. Lett.*, 2013, **103**, 111115-111118.
30 J. Zhang and A. Zayats, *Opt. Express*, 2013, **21**, 8426-8436.
31 J. Wang, C. Fan, J. He, P. Ding, E. Liang and Q. Xue, *Opt. Express*, 2013, **21**, 2236-2244.
32 Y. Zhang, T. Q. Jia, H. M. Zhang and Z. Z. Xu, *Opt. Lett.*, 2012, **37**, 4919-4921.
33 A. D. Khan, S. D. Khan, R. U. Khan and N. Ahmad, *Plasmonics*, 2014, **9**, 461.
34 L.Y. Yin, Y. H. Huang, X. Wang, S. T. Ning and S. D. Liu, *AIP Advances*, 2014, **4**, 077113.
35 N. Liu, M. Hentschel, T. Weiss, A. P. Alivisatos and H. Giessen, *Science*, 2011, **332**, 1407-1410.
36 A. Artar, A. A. Yanik and H. Altug, *Nano Lett.*, 2011, **11**, 3694-3700.
37 L. V. Brown, H. Sobhani, J. B. Lassiter, P. Nordlander and N. J. Halas, *ACS Nano*, 2010, **4**, 819–832.
38 Z. J. Yang, Z. S. Zhang, L. H. Zhang, Q. Q. Li, Z. H. Hao and Q. Q. Wang, *Opt. Lett.*, 2011, **36**, 1542–1544.
39 N. Liu, H. C. Guo, L. W. Fu, S. Kaiser, H. Schweizer and H. Giessen, *Nat. Mater.*, 2008, **7**, 31−37.
40 N. Liu and H. Giessen, *Angew. Chem. Int. Ed*, 2010, **49**, 9838−9852.
41 J. D. Jackson, *Classical Electrodynamics*, John Wiley & Sons, Inc., 1999.
42 N. Verellen, P. Van Dorpe, C. Huang, K. Lodewijks, G. A. E. Vandenbosch, L. Lagae and V. V. Moshchalkov, *Nano Lett.*, 2011, **11**, 391-397.
43 N. Verellen, P. Van Dorpe, D. Vercruysse, G. A. E. Vandenbosch and V. V. Moshchalkov, *Opt. Express*, 2011, **19**, 11034-11051.
44 S. A. Maier, P. G. Kik, H. A. Atwater, S. Meltzer, E. Harel, B. E. Koel and A. A. G. Requicha, *Nat. Mater.*, 2003, **2**, 229−232.
45 M. L. Brongersma, J. W. Hartman and H. A. Atwater, *Phys. Rev. B*, 2000, **62**, R16356.
46 W. H. Weber and G. W. Ford, *Phys. Rev. B*, 2004, **70**, 125429.
47 P. B. Johnson and R. W. Christy, *Phys. Rev. B*, 1972, **6**, 4370−4379.

(a)

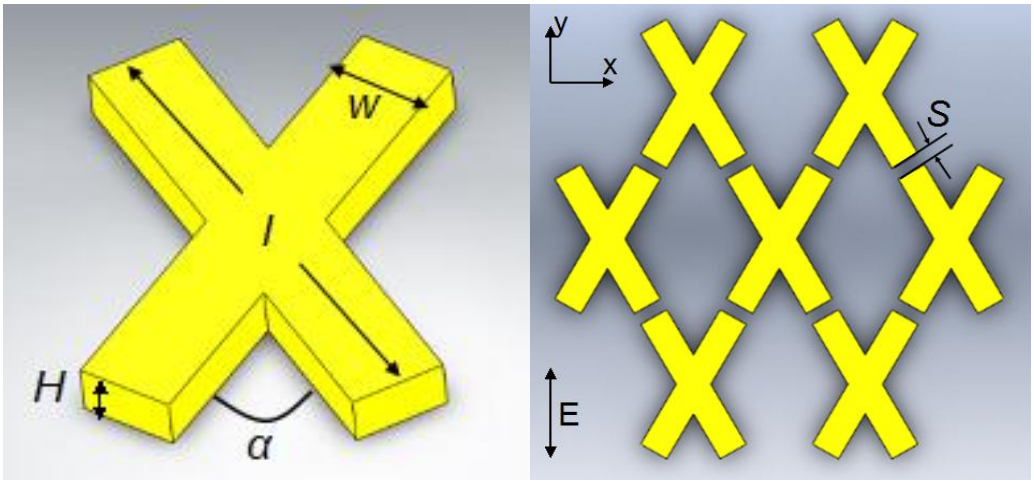

(b)

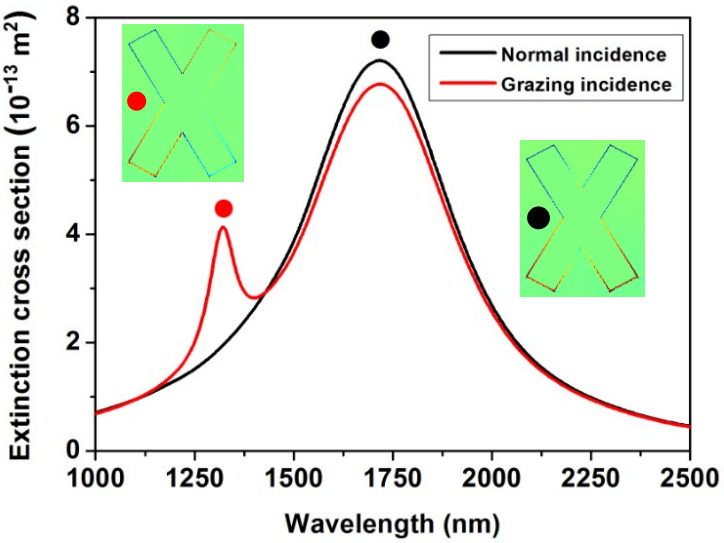

Fig. 1 (a) Schematic diagram of the plasmonic heptamer structure (right) consisting of seven nanocrosses (left) with definition of the geometrical parameters: l = 370 nm, W = 70 nm, H = 50 nm, α = 60 ° and S = 30 nm. (b) Calculated extinction spectra for a single nanocross illuminated by a y-polarized plane wave from the top (black line) and the side (red line). Insets: calculated charge density distribution of the dipolar (black dot) and quadrupolar mode (red dot).

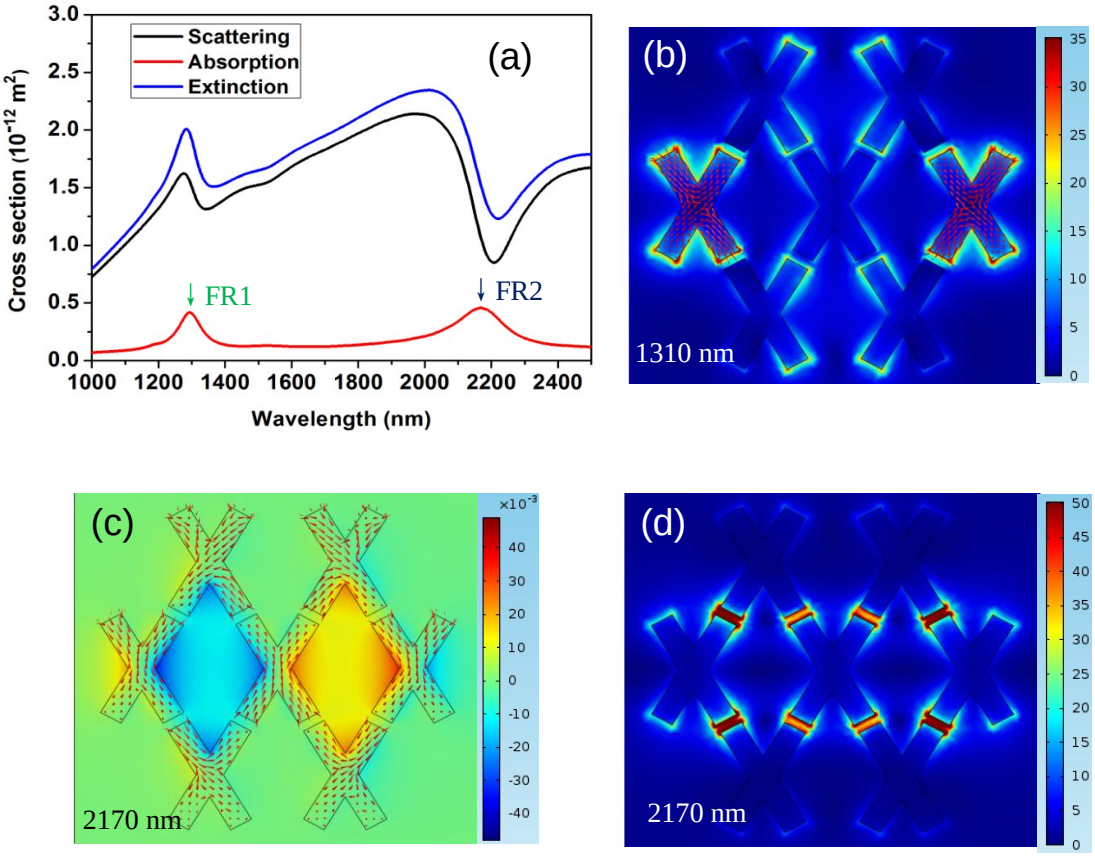

Fig. 2 (a) Extinction, scattering and absorption cross section spectra of the heptamer structure as shown in Fig. 1(a). The electric field enhancement distributions corresponding to the position of FR1 (1310 nm) and FR2 (2170 nm) on the absorption spectrum are demonstrated in (b) and (d), respectively. The electric field at resonance FR1 is mostly localized on the left and right side nanocross, and the dominant plasmonic mode is revealed in the superimposed current vector distributions. (c) Current vector distributions superimposed with the magnetic field at resonance FR2. The antiphase ring currents can be observed obviously.

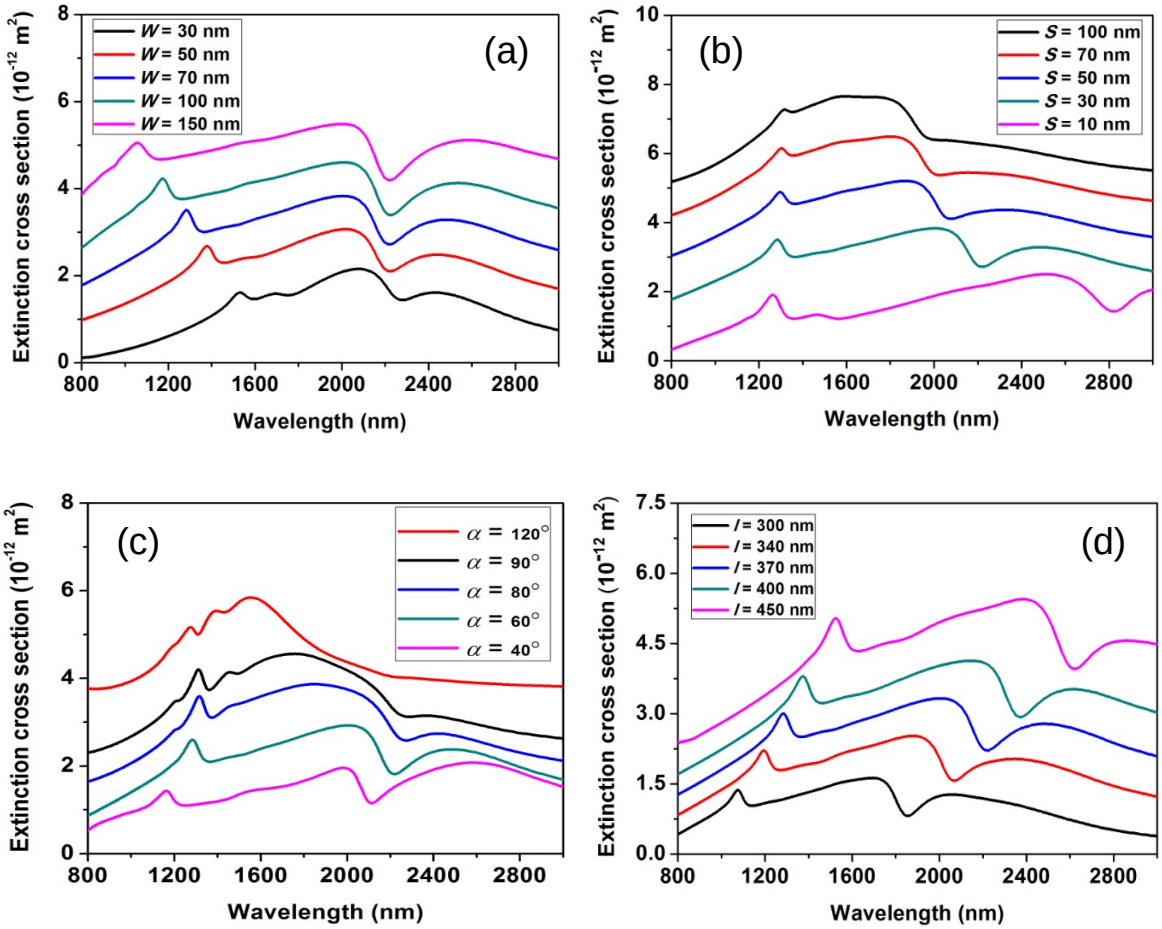

Fig. 3 Extinction cross section spectra as a function of the nanocross arm width *W*, the gap between neighbor nanocrosses *S*, the angle α and the arm length *l*, respectively. (a) *l* =370 nm, *S* = 30 nm, *H* = 50 nm and α = 60 °. (b) *l* =370 nm, *W* = 70 nm, *H* = 50 nm and α = 60 °. (c) *l* =370 nm, *W* = 70 nm, *H* = 50 nm and *S* = 30 nm. (d) *W* = 70 nm, *H* = 50 nm and α = 60 °. The distance between the ends of the adjacent arms is kept at 30 nm. Spectra are shifted upward for clarity.

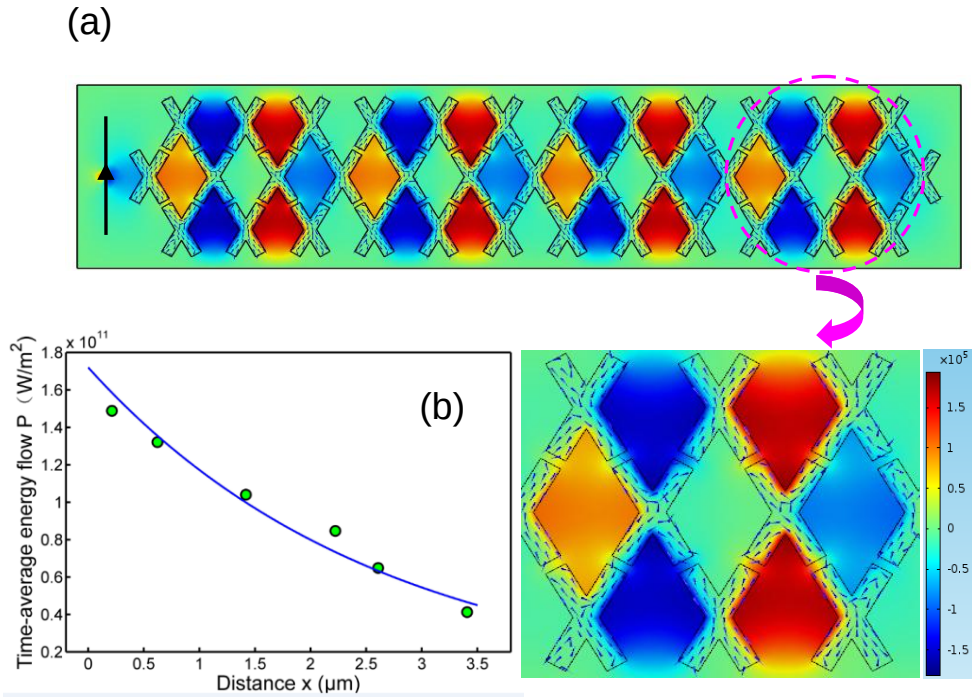

Fig. 4 (a) Magnetic field plots superimposed with current vector distributions of a coupled chain with twelve tetramer units at the selected resonant wavelength (2030 nm) using a electric dipole excitation source. The dipole source with an amplitude of 1×10^{-9} mA is placed at a distance of 150 nm from the left end of the chain (indicated by the dark arrow line). The bottom inset shows a zoomed-in part to clarify the current vectors. (b) The energy flow as a function of the distance along the chain. The tetramers at two ends are excluded in the fitting in order to avoid the influence of light scattering. The fitted energy flow equation is $P = 1.7197 \times 10^{11} \exp(-x/2.608)$, corresponding to a field decay length of 2.608 μm.